

Design and Control of a Novel Plane Maglev System Based on Analyzing Magnetic Force

Ming-Chiu Shiu^{a,c}, Mei-Yung Chen^a, Shin-Guang Huang^a and Li-Chen Fu^{a,b}

^aDepartment of Electrical Engineering, National Taiwan University

^bDepartment of Computer Science and Information Engineering
National Taiwan University

^{a,b}No.1, Sec.4, Roosevelt Road, Taipei 106, Taiwan, China

^bE-mail: lichen@ccms.ntu.edu.tw

^cDepartment of Electrical Engineering, Hsiuping Institute of Technology

^cNo.11, Gungye Road, Dali City, Taichung 412, Taiwan, China

E-mail: smc@mail.hit.edu.tw

Abstract - In this paper, a novel 6-DOF magnetic levitation (Maglev) system is proposed. As a result of using the cylindrical solenoid and rectangular coils as actuators, we thought analysis of magnetic forces inside the both kinds of coil form the main basis of designing our system. In this system, both new mechanical structure and adaptive control algorithm are developed. Structurally, totally there are eight permanent magnets (PMS) attached to the carrier, whereas there are eight coils respectively mounted on a fixed base. After analyzing the magnetic force characteristics between permanent magnets and coils, and detailed studied the general model of this system with full 6DOFs is therefore derived and analyzed. Next, an adaptive controller is developed for such a system to deal with the unknown parameters with the objective of precision positioning. From the experimental results, satisfactory performances including regulation accuracy and control stiffness have been demonstrated.

Index Terms - Magnetic force, Maglev, Permanent magnet, Adaptive controller..

I. INTRODUCTION

With the progress of the industrial technologies, the high-precision positioning system plays an important role in various high-tech fields. To meet these challenging needs, more stringent manufacturing processes and advanced fabrication equipments, therefore, should be developed. In traditional mechanical actuators, mostly the piezoelectric actuators [1][2] only handle the small moving range, the ball-screws cause disturbances and backlash due to roughness of the bearing elements [3][4], and linear motors have ripple effect in a motion stroke. It is generally believed that magnetic levitation system not only achieves advantages that the previous two actuators possess but even overcome their shortcomings as well.

Based on the design theories and experience for developing dual-axis Maglev guiding systems and planar maglev positioning system [5][6], a new planar Maglev system is proposed in this paper. There are eight PMs attached to the moving part, which is the so-called carrier, whereas there are eight coils respectively mounted on a fixed base. Four of these eight coils are arranged in the bottom, which

mainly generate levitating forces as well as torques around X- and Y-axis. On the other hand, the four lateral-coils with rectangle shaped mainly produce lateral forces and torque around Z-axis as well. The conceptual configuration and photograph of this system is shown in Fig. 1(a), Fig. 1(b) and Fig. 2, respectively.

In this paper, first, the magnetic force characteristics are analyzed. Then, the dynamic model with full 6DOFs is derived from it. Also, an adaptive controller that deals with unknown parameters is proposed to control the carrier at the desired target point. To demonstrate the performance of the entire system, experimental results are provided for verification. The organization of this paper is as follows. The detailed description of the complete dynamics that including the magnetic force characteristics will be given in Section II. And Section III concentrates on the system modelling and controller design. Section IV is about the experimental results as well as some discussions. Finally, conclusions are given in section V.



Fig. 1(a). The view of the carrier with eight embedded Permanent magnets



Fig. 1(b). The view of the coils in the platform



Fig. 2. Photograph of the planar Maglev system

II. MAGNETIC FORCE DISSECTING

About this system, it can be regarded composed of eight sub-systems. The upper four sub-systems and the lower four have different pairs of coil and PM. They are rectangular and cylindrical, respectively. To model this system, the interactions between coil and PM become a very important issue. Thus in this section we begin with two approaches, which are introduced to analyze these interactions. Furthermore, this modeling result will then be integrated to develop the general model of the hereby proposal.

A. Analysis of Magnetic Force Characteristics

First, we try to model the interactions from the analytic approach by utilizing several useful fundamental theorems in electromagnetics. The force \vec{F} and torque \vec{T} exerted on a PM, which is exposed in an external magnetic field \vec{H} , can be obtained from the *Lorentz force form*

$$\vec{F} = (\vec{m} \cdot \nabla) \mu_0 \vec{H}, \quad (1)$$

$$\vec{T} = \vec{m} \times (\mu_0 \vec{H}). \quad (2)$$

where \vec{m} denotes the dipole moment of the PM and μ_0 is the permeability of free space which is equal to $4\pi \times 10^{-7}$ (H/m). In this system, it is assumed that each PM can be viewed as a single magnetic dipole moment with the direction perpendicular to its surface. Therefore, how to derive the magnetic field \vec{H} becomes an important task in this research.

From *Biot-Savart Law* [7], the magnetic field \vec{H} can be expressed as:

$$\vec{H} = \frac{1}{4\pi} \int \frac{\vec{J}(\vec{r}') \times \vec{i}_{r,r'}}{|\vec{r} - \vec{r}'|^2} dv'. \quad (3)$$

where \vec{J} is the current density, \vec{r}' is the source coordinate, \vec{r} represents the observer coordinate, $\vec{i}_{r,r'}$ is a unit vector directed from \vec{r}' to \vec{r} , and dv' is a infinitesimal cube of the current source.

B. Magnetic Field Inside the Coi

Generally speaking, we need to have sufficient understanding about the property of every element device before we can assemble them into our MagLev system. What is shown in Fig. 3 is a rectangular coil with inner-length a , inner-width b , height h and current I (≈ 1 A). Apparently, the origin of the coordinate attached to the coil is at the center of the coil's bottom.

First of all, we should explore the property of the magnetic field inside the coil. By using an auxiliary software,

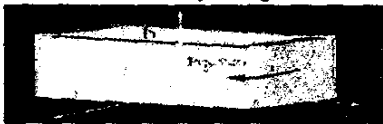


Fig. 3. Coordinate and dimension of a rectangle coil

we can perform 3D-simulation of the magnetic field on the xy -plane at $z=0.01$ meter or at $z=0.0245$ meter over the range ($x:-0.025 \rightarrow 0.025$ meter, $y:-0.025 \rightarrow 0.025$ meter), where B_x means the part of B in the x -direction, B_y means the part of B in the y -direction, B_z means the part of B in the z -direction, and the unit of the magnetic flux (B) is Gauss.

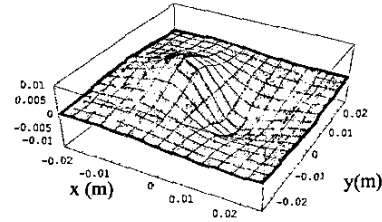


Fig. 4. B_x in the xy -plane ($z=0.01$ meter)

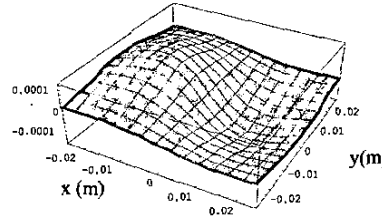


Fig. 5. B_x in the xy -plane ($z=0.0245$ meter)

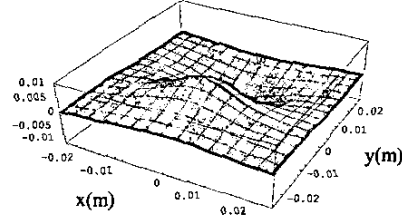


Fig. 6. B_y in the xy -plane ($z=0.01$ meter)

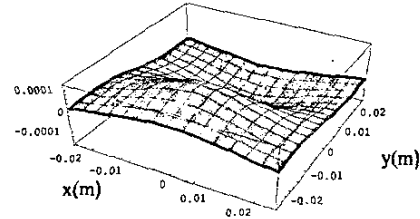


Fig. 7. B_y in the xy -plane ($z=0.0245$ meter)

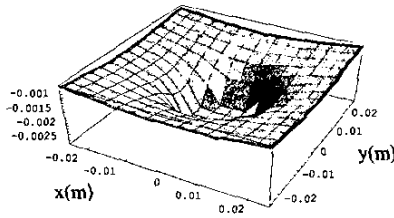


Fig. 8. B_z in the xy -plane ($z=0.01$ meter)

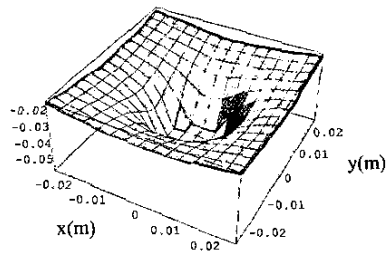


Fig. 9. B_z in the xy -plane ($z=0.0245$ meter)

TABLE I
THE COMPARISONS OF B IN THE POSITION INSIDE THE COIL

| Z (xy-plane) | 0(bottom) | 0.01m | 0.025m(center) | 0.04m | 0.05m(top) |
|--------------|-----------|-------|----------------|-------|------------|
| B_x | High | ← | Low | → | High |
| B_y | High | ← | Low | → | High |
| B_z | Low | → | High | ← | Low |

According to the results of Fig. 4□ 9, we can obtain the characteristics of the magnetic field in the space inside the coil as shown in Table I.

After looking up the Table I, we can find that the minimum of B_x (B_y) and the maximum of B_z occur at the center of the coil. In fact, both rectangular coil and cylindrical solenoid will have similar property in magnetic field distribution. These results of simulation are very similar to the actual physical phenomenon.

C. Magnetic Force inside the Coil

In this section, we will investigate the magnetic force F (NT) of a dipole moment m ($=1.5 \text{ Am}^2$) inside the coil. We also acquire the 3D numerical distribution of the magnetic force on the xy -planes at $z=0.01$ meter or at $z=0.0245$ meter over the range ($x: -0.025 \rightarrow 0.025$ meter, $y: -0.025 \rightarrow 0.025$ meter), where F_x means the component of F in the x -direction, F_y means the component of F in the y -direction, and F_z means the component of F in the z -direction.

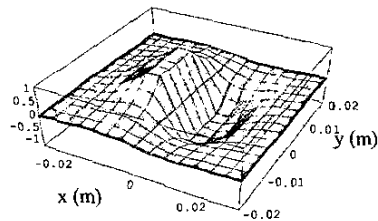


Fig. 10. F_x in the xy -plane ($z=0.01$ meter)

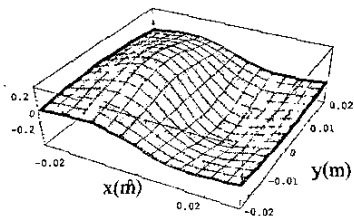


Fig. 11. F_x in the xy -plane ($z=0.0245$ meter)

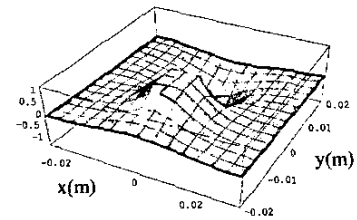


Fig. 12. F_y in the xy -plane ($z=0.01$ meter)

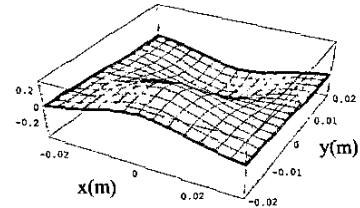


Fig. 13. F_y in the xy -plane ($z=0.0245$ meter)

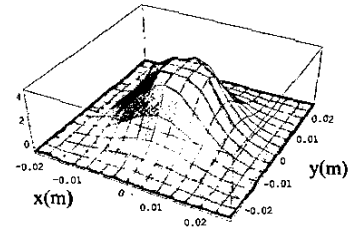


Fig. 14. F_z in the xy -plane ($z=0.01$ meter)

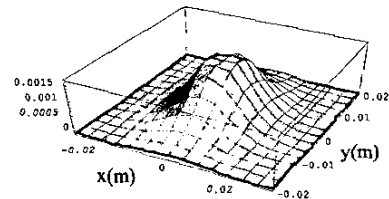


Fig. 15. F_z in the xy -plane($z=0.0245$ meter)

On the other hand, we can extract more important meanings from the force simulations by investigating the force distribution on the xz -planes at $y=0$ meter over the range ($x: -0.03 \rightarrow 0.03$ meter, $z: 0.01 \rightarrow 0.04$ meter, $m=1.5 \text{ Am}^2$, $I=1A$) as shown in Fig. 16 and 17. It can be found that when the location of PM is above or below the center of coil, it will be attracted to the center referring to Fig. 16. In summary, the pair of the coil and a PM has a stable equilibrium point at the center of the coil under the following conditions:

1. if the vector of dipole moment (m) is in the $+z$ direction, and I is in the counterclockwise direction;
2. if the vector of dipole moment (m) is in the $-z$ direction, and I is in the clockwise direction.

But when the location of PM is above or below the center of coil, it will be repelled away the center referring to Fig. 17.

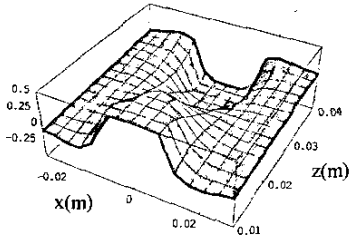


Fig. 16. Fz in the xz-plane (y=0meter)

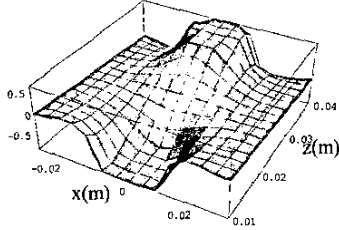


Fig. 17. Fz in the xz-plane (y=0meter)

To sum up, the pair of a coil and a PM has an unstable equilibrium point at the center of coil under the following conditions:

1. if the vector of dipole moment (m) is in the $-z$ direction, and I is in the counterclockwise direction;
2. if the vector of dipole moment (m) is in the $+z$ direction, and I is in the clockwise direction.

In our developed system, we will set up the positioning force and levitation force exerted to the carrier basically using repulsion mechanism as will be explained in the following:

Here, four PMs embedded at the bottom of the carrier are used to counteract the weight of the carrier. But, besides the levitation forces there will be unstable lateral forces (F_x, F_y) coming along to make the carrier statically unstable in the lateral direction. So, we design the carrier such that there is a PM embedded in the foot plate of each extended bar and the total four PMs together with the rectangular coils will sufficiently provide the lateral control forces to hold the carrier still. In this Maglev positioning system, generation of levitation forces will usually be at the price of destabilization in lateral directions (when the carrier is not right at the equilibrium state).

After we have carefully described the mechanism of the Maglev system, what is left for us is to develop an appropriate control, which not only can levitate the carrier but also will position the carrier precisely at the pre-specified location or will move it following the desired speed and trajectory.

III. SYSTEM MODELING

In order to realize such high-precision positioning system, we must control not only the translation but also the attitude of the carrier. To this end, a complete analytical model will be derived first, which includes two lateral DOFs, one propulsion DOF and three attitude DOFs. Before we derive the model, several technical assumptions must be made.

Assumptions:

1. Every PM (permanent magnet) is considered as one single dipole carrying the same magnetic dipole moment and is located at the center of each PM.
2. These PMs do not have any influence among one another.
3. These coils are arranged such that the mutual inductance among them can be negligible.
4. Both the carrier and platform are rigid bodies.

After these assumptions are validated, the complex analysis of the overall MagLev system will become simpler.

A. Controller Design and Stability Analysis

To simplify our notations from here on, we will drop the differential symbol “ δ ” and abuse the notations by identifying the variable δX with X and doing the same to all others. Under this circumstance, we further redefine the control inputs $u_1 \dots u_8$ as $u_1 = I_A, u_2 = I_B, u_3 = I_C, u_4 = I_D, u_5 = I_E, u_6 = I_F, u_7 = I_G, u_8 = I_H$. As a result of this notational simplification, the plant model now becomes:

$$\begin{aligned}
 \ddot{X} &= K_{1X}X + K_{1Y}Y + K_{1Z}Z + K_{1\psi}\psi + K_{1\phi}\phi + K_{1\theta}\theta + K_{1A}u_1 \\
 &\quad + K_{1B}u_2 + K_{1C}u_3 + K_{1D}u_4 + K_{1E}u_5 + K_{1F}u_6 + K_{1G}u_7 \\
 &\quad + K_{1H}u_8 \\
 \ddot{Y} &= K_{2X}X + K_{2Y}Y + K_{2Z}Z + K_{2\psi}\psi + K_{2\phi}\phi + K_{2\theta}\theta + K_{2A}u_1 \\
 &\quad + K_{2B}u_2 + K_{2C}u_3 + K_{2D}u_4 + K_{2E}u_5 + K_{2F}u_6 + K_{2G}u_7 \\
 &\quad + K_{2H}u_8 \\
 \ddot{Z} &= K_{3X}X + K_{3Y}Y + K_{3Z}Z + K_{3\psi}\psi + K_{3\phi}\phi + K_{3\theta}\theta + K_{3A}u_1 \\
 &\quad + K_{3B}u_2 + K_{3C}u_3 + K_{3D}u_4 + K_{3E}u_5 + K_{3F}u_6 + K_{3G}u_7 \\
 &\quad + K_{3H}u_8 \\
 \ddot{\psi} &= K_{4X}X + K_{4Y}Y + K_{4Z}Z + K_{4\psi}\psi + K_{4\phi}\phi + K_{4\theta}\theta + K_{4A}u_1 \\
 &\quad + K_{4D}u_4 + K_{4E}u_5 + K_{4F}u_6 + K_{4G}u_7 + K_{4H}u_8 \\
 \ddot{\phi} &= K_{5X}X + K_{5Y}Y + K_{5Z}Z + K_{5\psi}\psi + K_{5\phi}\phi + K_{5\theta}\theta + K_{5A}u_1 \\
 &\quad + K_{5C}u_3 + K_{5E}u_5 + K_{5F}u_6 + K_{5G}u_7 + K_{5H}u_8 \\
 \ddot{\theta} &= K_{6X}X + K_{6Y}Y + K_{6Z}Z + K_{6\psi}\psi + K_{6\phi}\phi + K_{6\theta}\theta + K_{6A}u_1 \\
 &\quad + K_{6B}u_2 + K_{6C}u_3 + K_{6D}u_4
 \end{aligned} \tag{4}$$

Note that all the above resulting linear coefficients can be found in [8].

B. Adaptive Controller Design

After we take into account the calibration error of sensors in our final plant model, (4) can be rewritten as:

$$\begin{bmatrix} \ddot{X} \\ \ddot{Y} \\ \ddot{Z} \\ \ddot{\psi} \\ \ddot{\phi} \\ \ddot{\theta} \end{bmatrix} = \begin{bmatrix} K_{1X} & K_{1Y} & K_{1Z} & K_{1\psi} & K_{1\phi} & K_{1\theta} \\ K_{2X} & K_{2Y} & K_{2Z} & K_{2\psi} & K_{2\phi} & K_{2\theta} \\ K_{3X} & K_{3Y} & K_{3Z} & K_{3\psi} & K_{3\phi} & K_{3\theta} \\ K_{4X} & K_{4Y} & K_{4Z} & K_{4\psi} & K_{4\phi} & K_{4\theta} \\ K_{5X} & K_{5Y} & K_{5Z} & K_{5\psi} & K_{5\phi} & K_{5\theta} \\ K_{6X} & K_{6Y} & K_{6Z} & K_{6\psi} & K_{6\phi} & K_{6\theta} \end{bmatrix} \begin{bmatrix} X \\ Y \\ Z \\ \psi \\ \phi \\ \theta \end{bmatrix} + \begin{bmatrix} K_{1A} & K_{1B} & K_{1C} & K_{1D} & K_{1E} & K_{1F} & K_{1G} & K_{1H} \\ K_{2A} & K_{2B} & K_{2C} & K_{2D} & K_{2E} & K_{2F} & K_{2G} & K_{2H} \\ K_{3A} & K_{3B} & K_{3C} & K_{3D} & K_{3E} & K_{3F} & K_{3G} & K_{3H} \\ 0 & K_{4B} & 0 & K_{4D} & K_{4E} & K_{4F} & K_{4G} & K_{4H} \\ K_{5A} & 0 & K_{5C} & 0 & K_{5E} & K_{5F} & K_{5G} & K_{5H} \\ K_{6A} & K_{6B} & K_{6C} & K_{6D} & 0 & 0 & 0 & 0 \end{bmatrix} \begin{bmatrix} u_1 \\ u_2 \\ u_3 \\ u_4 \\ u_5 \\ u_6 \\ u_7 \\ u_8 \end{bmatrix} + \begin{bmatrix} g_1 \\ g_2 \\ g_3 \\ g_4 \\ g_5 \\ g_6 \end{bmatrix} \quad (5)$$

and hence (5) can also be modified accordingly as:

$$\ddot{E} = AE + BU + g \quad (6)$$

where $E = [X \ Y \ Z \ \psi \ \phi \ \theta]^T$, $U = [u_1 \ u_2 \ u_3 \ u_4 \ u_5 \ u_6 \ u_7 \ u_8]^T$ and $g = [g_1 \ g_2 \ g_3 \ g_4 \ g_5 \ g_6]^T$. Note that E, U and g are the state vector, input vector, and calibration errors, respectively. Our control objectives here are to regulate the error signals E into zero values by devising the control U properly. However, due to lack of knowledge of the system parameters, we assume A, B and g are unknown except the sign of each element in B . Thus, the control law is chosen as:

$$U = \hat{B}^{-1}[-\hat{A}E - \hat{g} - D\dot{E} - PE] \quad (7)$$

Then, the closed-loop system after (8) is substituted into (6) becomes

$$\ddot{E} + D\dot{E} + PE = \tilde{A}E + \tilde{B}U + \tilde{g} \quad (8)$$

where the estimation error $\tilde{A} = A - \hat{A}$, $\tilde{B} = B - \hat{B}$ and $\tilde{g} = g - \hat{g}$. To achieve the control objective, we define a sliding surface vector S as:

$$S = \dot{E} + \Lambda_1 E \quad (9)$$

which being substituted into (8) leads to:

$$\dot{S} + \Lambda_2 S = \tilde{A}E + \tilde{B}U + \tilde{g} \quad (10)$$

where $S = [s_1 \ s_2 \ s_3 \ s_4 \ s_5 \ s_6]$, and both $\Lambda_1 = \text{diag}(\lambda_1, \lambda_2, \dots, \lambda_6)$ and $\Lambda_2 = \text{diag}(\lambda'_1, \lambda'_2, \dots, \lambda'_6)$ are positive definite matrices.

C. Stability Analysis

To find out the adaptive law, we first define a Lyapunov function candidate V as follows:

$$V = \frac{1}{2} S^T S + \frac{1}{2} \text{tr}[(\tilde{A})^T G_A^{-1} (\tilde{A})] + \frac{1}{2} \text{tr}[(\tilde{B})^T G_B^{-1} (\tilde{B})] + \frac{1}{2} \text{tr}[(\tilde{g})^T G_g^{-1} (\tilde{g})] \quad (11)$$

where G_A, G_B and G_g are all positive definite diagonal matrices. To assess the boundedness as well as convergence of all the involved errors, we will try to evaluate the time derivative of the function V in the following:

$$\dot{V} = S^T \dot{S} + \text{tr}[(\tilde{A})^T G_A^{-1} (\dot{\tilde{A}})] + \text{tr}[(\tilde{B})^T G_B^{-1} (\dot{\tilde{B}})] + \text{tr}[(\tilde{g})^T G_g^{-1} (\dot{\tilde{g}})] \quad (12)$$

Substitute S from (9) into (12) to yield

$$\begin{aligned} \dot{V} &= S^T [\tilde{A}E + \tilde{B}U + \tilde{g} - \Lambda_2 S] + \text{tr}[(\tilde{A})^T G_A^{-1} (\dot{\tilde{A}})] \\ &\quad + \text{tr}[(\tilde{B})^T G_B^{-1} (\dot{\tilde{B}})] + \text{tr}[(\tilde{g})^T G_g^{-1} (\dot{\tilde{g}})] \\ &= -S^T \Lambda_2 S + S^T \tilde{A}E + S^T \tilde{B}U + S^T \tilde{g} + \text{tr}[(\tilde{A})^T G_A^{-1} (\dot{\tilde{A}})] \\ &\quad + \text{tr}[(\tilde{B})^T G_B^{-1} (\dot{\tilde{B}})] + \text{tr}[(\tilde{g})^T G_g^{-1} (\dot{\tilde{g}})] \end{aligned} \quad (13)$$

So that, the obvious choice for $\dot{\tilde{A}}$, $\dot{\tilde{B}}$ and $\dot{\tilde{g}}$ to make \dot{V} negative is

$$\begin{aligned} \dot{\tilde{A}} &= -\dot{\tilde{A}} = G_A S E^T, \text{ where } G_A = \text{diag}(\chi_{A1}, \chi_{A2}, \dots, \chi_{A6}) \\ \dot{\tilde{B}} &= -\dot{\tilde{B}} = G_B S U^T, \text{ where } G_B = \text{diag}(\chi_{B1}, \chi_{B2}, \dots, \chi_{B6}) \\ \dot{\tilde{g}} &= -\dot{\tilde{g}} = G_g S, \text{ where } G_g = \text{diag}(\chi_{g1}, \chi_{g2}, \dots, \chi_{g6}), \end{aligned}$$

so that (13) can be further simplified as:

$$\dot{V} = -S^T \Lambda_2 S \leq 0 \quad (14)$$

Based on (11) and (14) and according to the Lyapunov stability theory, we can conclude that S, \tilde{A}, \tilde{B} and \tilde{g} are all bounded, and $S \in L_2$. Referring to (10), we can find that $\dot{S} \in L_\infty$ and hence S is uniformly continuous, which together with the fact that $S \in L_2$ will readily imply that $|S| \rightarrow 0$ as $t \rightarrow \infty$ by Barbalat's Lemma [9]. It is, however, worth mentioning that \hat{A} , \hat{B} and \hat{g} may not converge to their true values A , B and g . Of course, if the so-called persistent excitation (PE) condition can be satisfied, estimates should be able to converge to their true values asymptotically. Under that circumstance, the input command U readily becomes what we derive as if all the parameters were known. Regardless of the failure of parameter convergence, the error E and \dot{E} will approach to zero asymptotically. In other words, six state

errors and their time derivatives will all converge to zero asymptotically. As a consequence, the objective in our developed system can be fulfilled by the formerly designed controller.

IV. EXPERIMENT RESULTS

The experiment hardware, including the main body, sensor system, driver system and controller hardware, will be described here. A number of experiment results, including the regulation and positioning will also be provided in this section to demonstrate performance of this system with the controller presented in section III.

In our experiment results as Fig.18~29, not only the performance of regulation but also the positioning has been achieved as desired goals. Besides, all the states will converge to their desired values with precision, and these experiment results are quite consistent with the results from numerical simulations.

Finally, the regulation and positioning errors are within $100\ \mu\text{m}$, which are yet to be further improved.

V. CONCLUSION

In this paper, we proposed a novel planar Maglev positioning system. This maglev system can be readily used in a clean room, since it will not generate wearing particles and no lubrication is required. Furthermore, there is no mechanical contact between the moving part and the stators. This design is also highly suitable for vacuum environments, since the heat generated in the motors in the fixed frame.

Then, the dynamics of our Maglev system have been thoroughly analyzed and its mathematical model with complete six DOFs (degree-of freedoms) is also detailed derived. By this, we can particularly understand the dynamics between a levitated free body and platform of guiding system.

The system is treated as a MIMO system, and an adaptive controller has been designed to regulate the six DOFs to a precision extent. Finally, satisfactory performance of precision positioning motion can be obtained in the actual experiments. The inexact setup of mechanism and the inaccurate precision of sensors will result in the error in our system performance. Based on the process of experiment, we find that the improvement of system performance is possible if the more high-precision sensors, the exacter mechanism and the more advanced control is practiced.

The hereby-developed Maglev planar positioning system is novel in that it can provide planar dual-axis motion capability, which involves only pure magnetic forces. Functionally, such mechanism behaviors just like a planar XY table with high precision.

To sum up, a high-precision novel planar Maglev positioning system has been successfully put into practice there.

ACKNOWLEDGMENT

This research is sponsored by National Science Council, Taiwan, China, under the grant no. NSC-90-2213-E-003-054.

REFERENCES

- [1] Sitti, M. and Hashimoto, H., "Two-dimensional fine particle positioning using a piezoresistive cantilever as a micro/nano-manipulator", 1999 *IEEE International Conference on Robotics and Automation*, Vol. 4, 1999, pp. 2729–2735.
- [2] Hector M. Gutierrez, Paul I. Ro. "Sliding-Mode Control of a Nonlinear-Input System: Application to a Magnetically Levitated Fast-Tool Servo", *IEEE Tran. on Industrial Electronics*, Vol. 45, no. 6, 1998, pp. 921–927.
- [3] Li Xu and Bin Yao, "Adaptive robust precision motion control of linear motors with negligible electrical dynamics: theory and experiments", *IEEE/ASME Tran. on Mechatronics*, Vol. 6 Issue: 4, 2001, pp. 444–452.
- [4] Pai-Yi Huang, Yung-Yew Chen and Min-Shin Chen "Position-dependent friction compensation for ballscrew tables", *Proceedings of the 1998 IEEE International Conference on Control Applications*, Vol. 2, 1998, pp. 863–867.
- [5] Chen, M. Y., Wu, K. N. and Fu, L. C., "Design, Implementation and Self-tuning Adaptive Control of a Maglev Guiding System", *Mechatronic*, 2000, pp. 215-237.
- [6] Shiu, M. C.;" Design and Control of a Novel Planar Maglev Positioning System." Master thesis. The National Taiwan University, Taiwan, China, 2001.
- [7] David, J. G., *Introduction to Electrodynamics*. Prentice-Hall, Inc., Englewood Cliffs, New Jersey, 1981.
- [8] Huang, S. G.;" Design Control and Experiment of a Novel Precise Maglev Positioning System." Master thesis. The National Taiwan University, Taiwan, China, 2002.
- [9] Jean-Jacques E. Slotine, Weiping Li., *Applied nonlinear control*, Prentice Hall, 1990.

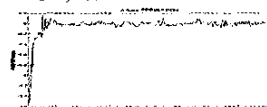


Fig.18. Regulation response on X-axis.



Fig.19. Regulation response on Y-axis

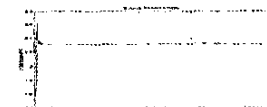


Fig.20. Regulation response on Z-axis.



Fig.21. Pitch Regulation

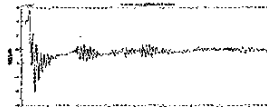


Fig.22. Yaw regulation.



Fig.23. Roll regulation

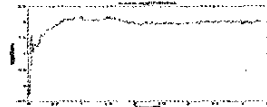


Fig.24. Positioning response on X-axis.

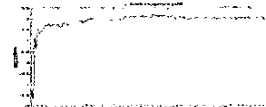


Fig.25. Positioning response on Y-axis

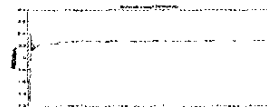


Fig.26. Positioning response on Z-axis.

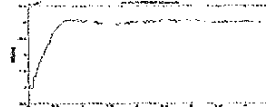


Fig.27. Positioning response for pitch



Fig.28. Positioning response for yaw.



Fig.29. Positioning response for roll